Lab on a Chip

RSC Publishing

PAPER
Charles N. Baroud *et al.*
Parallel measurements of reaction kinetics using ultralow-volumes

Parallel measurements of reaction kinetics using ultralow-volumes†

Etienne Fradet,[a] Paul Abbyad,‡[b] Marten H. Vos[b] and Charles N. Baroud*[a]

We present a new platform for the production and manipulation of microfluidic droplets in view of measuring the evolution of a chemical reaction. Contrary to existing approaches, our device uses gradients of confinement to produce a single drop on demand and guide it to a pre-determined location. In this way, two nanoliter drops containing different reagents can be placed in contact and merged together, in order to trigger a chemical reaction. The reaction rate is extracted from an analysis of the observed reaction–diffusion front. We show that the results obtained using this platform are in excellent agreement with stopped-flow measurements, while decreasing the sample consumption 5000 fold. We also show how the device operation can be parallelized in order to react an initial sample with a range of compounds or concentrations, on a single integrated chip. This integrated chip thus further reduces sample consumption while reducing the time required for the experimental runs from hours to minutes.

Recent years have witnessed rapid progress of droplet microfluidic methods for chemical and biological analysis,[1–3] which has led to applications for DNA analysis,[4,5] cell manipulation,[6] or other biological or biochemical advances.[3,7] Most of this work has focused on high-throughput applications that require 10^3–10^6 droplets, leading to the development of many tools for the formation and transport of such drops, in addition to methods for measuring their contents. These developments have already led to a new way of thinking about biological systems, through the emergence of "digital biology" where an initial sample is separated into compartments that provide a binary (*yes* or *no*) answer.[4]

An alternative approach is to extract more detailed information from a single droplet by observing variations of its contents in time, for instance to observe the evolution of a chemical reaction[8,9] or the response of a small number of cells to a stimulus.[10,11] Tools that address this low-throughput niche have been developed in the surface-actuated microfluidics approach, either through electrowetting[12] or through surface acoustic waves,[13] but they have remained very underdeveloped in microchannels. So although the volumes required to perform the measurement are small, a large part of the sample is wasted due to fluid handling limitations. This can be an important drawback when expensive or rare samples are used or when many different reactions are required.

Part of the difficulty of working with few drops comes from the classical methods of droplet generation and transport, which rely on stable flow rates at a flow-focusing or T-junction to produce the drops.[14] This implies that the initial drop production, before the fluid flows have reached a steady state, is poorly controlled. Recently however, gradients of confinement were introduced for the production and transport of drops without the need for a flow of the outer fluid and without any transient effects.[15] Two individual drops could therefore be produced on demand and brought together to merge and react, by only relying on the channel geometry, using a technique called "rails and anchors".[11]

Here we demonstrate a robust and easy to fabricate microfluidic platform that will allow such measurements to become routine. In particular, we show how chemical kinetics can be extracted from a single fusion of two nanoliter droplets and how the device can be parallelized to perform multiple independent reactions on an integrated chip. A simplified analysis method is introduced to measure the chemical kinetics and the results compare favorably with measurements obtained from a commercial stopped-flow machine, while requiring only a tiny fraction of the reagents.

The device consists of a square test section connected to four inlet channels of smaller width and height, two for oil and two for aqueous solutions, as shown on Fig. 1a. In addition, a goggle-like pattern, of larger height, is etched on top of the test section. This multilevel structure (Fig. 1b) is micro-fabricated using simple multi-layer dry film soft lithography.[16,17] In this

[a] Laboratoire d'Hydrodynamique (LadHyX) and Department of Mechanics, Ecole Polytechnique, CNRS, 91128, Palaiseau, France. E-mail: baroud@ladhyx.polytechnique.fr
[b] Laboratoire d'Optique et Biosciences (LOB), Ecole Polytechnique, INSERM U696, CNRS, 91128, Palaiseau, France
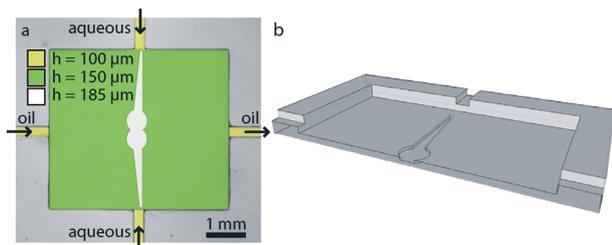
Fig. 1 (a) Top-down view of the test section. It consists of three regions of different heights h: four inlet channels, the test section in green, and the goggle pattern in white. (b) Perspective view of half the reaction chamber.

Fig. 2 Channel operation showing the reduction of DCPIP to a colorless molecule by L-ascorbic acid. (a) Injection of the DCPIP. (b) Injection of the L-ascorbic acid. (c) Static pair of touching droplets. An infrared laser pulse (wavelength $\lambda = 1480$ nm, power $P \sim 150$ mW), lasting 200 ms, is focused near the droplet–droplet interface to trigger coalescence. The laser is removed before coalescence starts. (d–e) Reactive front propagating along the fused droplet. The arrow indicates the line over which the time evolution is measured.

method, successive layers of solid photoresist are deposited and exposed to UV using a succession of masks that determine the features at each height. Once all layers are deposited and exposed, the complete device is developed to reveal the mold that is then used to produce PDMS devices. This procedure is rapid (few minutes) and simple to implement; it does not require a mask aligner since it relies on superposing millimeter-scale structures. The geometry that is thus defined provides the three operations that must be performed on the drops: their production, propulsion and pairing.

During operation, the device is first filled with a fully wetting oil used as the continuous phase and the oil is kept stationary for the rest of the experiment. By pushing the aqueous solutions past the step into the test section, a drop detaches when it reaches a well-calibrated size, a technique known as step emulsification.[18] The drop size is determined by the height of the step and, to a lesser extent, the injection rate of the dispersed phase.[19] As a result, injecting the aqueous solution past the step allows the production, on demand, of a single droplet of desired volume.

In the experiments reported here, the drop that detaches is large enough to remain squeezed between the top and bottom walls and this vertical confinement makes droplets sensitive to channel height modulations.[11,15] Indeed, confined droplets have a larger surface energy than spherical unconstrained drops of identical volume. Since droplets tend to minimize their surface energy, they migrate towards regions of reduced confinement. Consequently, the V-shaped grooves in our device, corresponding to the arms of the goggle, passively propel droplets toward the center of the test section by gradually releasing their confinement. Finally, droplets coming from the two inlet channels are held against each other in adjacent anchors in the center of the test region. The shape of the anchors ensures that the two drops are touching.

Typical device operation is shown in Fig. 2 and accompanying movie S1, ESI.† The device is first filled with a mixture of perfluorinated oil (FC40, 3M Fluorinated) and a PEG based fluoro-surfactant[20] at 0.1% (w:w). Next, a solution of 2,6-dichlorophenolindophenol (DCPIP) is injected from the top injection channel and a drop detaches and comes to a rest in the central trap, after which a drop of L-ascorbic acid is generated in the same way from the bottom injection channel (Fig. 2a–b).
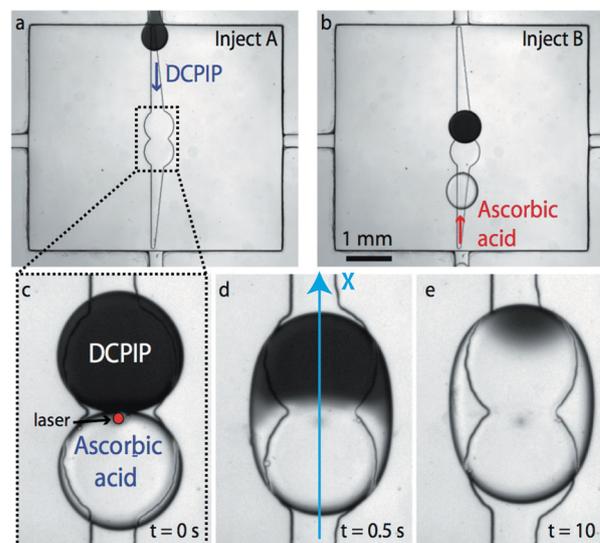
The two drops do not merge, due to the presence of the surfactant (Fig. 2c). However, a laser pulse on the touching interfaces triggers their fusion, which is initiated only after the laser has been removed,[17] and the fused drop quickly relaxes to the final oblong shape imposed by the anchors. The reaction starts immediately after fusion and a reactive front propagates in the fused drop, as shown in Fig. 2d–e, until the limiting reagent has been exhausted. Finally, once the reaction is completed, a transverse oil flux is used to remove the drop and reset the test section for another experiment.

In contrast to moving droplets where internal flows mix the reagents,[21–24] the reaction in the stationary drops takes place through a reaction–diffusion process.[9] In our devices, we match the drop sizes and interfacial tensions so that the contents remain well separated after the drop fusion. In the case when a drop of DCPIP (dark blue) is fused with a drop of buffer, the diffusion coefficient of the DCPIP can be measured ($D_B = 0.77 \times 10^{-9}$ m^2 s^{-1}) by following the spreading of the dye (see ESI† section 1 and movie S2). When the second drop contains the L-ascorbic acid, the reaction evolution can be modeled by a reaction–diffusion (R–D) set of equations with initially separated reagents.

We use the shorthand notation A for L-ascorbic acid, B for DCPIP and C for the reaction product. Since A and B are initially separated in two different droplets, they have to diffuse toward each other in order to react once the droplets merge. As a result, the local concentrations of A, B and C, noted [A], [B] and [C], are functions of both space and time. In addition, the reaction is known to follow second order kinetics[25] so the reaction rate is $R = k[A][B]$, which is also a function of space

and time. As a result, conservation laws for the three species yield:

$$\partial_t[A] = D_A\partial_{xx}[A] - k[A][B] \qquad (1)$$

$$\partial_t[B] = D_B\partial_{xx}[B] - k[A][B] \qquad (2)$$

$$\partial_t[C] = D_C\partial_{xx}[C] + k[A][B] \qquad (3)$$

where D_A, D_B and D_C are the diffusion coefficients of A, B and C, respectively (the model details are given in the ESI† section 2).

A and C being colorless, we are not able to measure their diffusion coefficients using brightfield images. Instead, we estimate them by comparing the molar weights of the molecules with B (see ESI† section 1). Then, the rate constant k is the only unknown parameter left in our model, which we therefore treat as a fitting parameter.

Eqn (1)–(3) are solved numerically for different reaction rate constants k and the numerical solution is compared with the measured profiles of B along the central axis of the daughter droplet (sketched by the x axis on Fig. 2d). The comparison is then used to obtain the value of k which makes the experimental and simulated profiles of B fit best for different times. A typical example is shown in Fig. 3a, where experimental profiles of DCPIP are superposed with their numerical best fits at four time points. Repeating the experiment for five initial concentrations A_0 yields $k = 83 \pm 4$ M^{-1} s^{-1}.

While this method yields a value of the reaction rate, it relies on image fitting techniques. A simpler approach is to monitor the total amount of B in the fused droplet over time ($\bar{B}$). This reduces the problem to fitting a time series of a single variable whose evolution integrates the effects of both diffusion and reaction. Three representative fits are shown in Fig. 3b, where the solid line is a fit to the experimental data based on the integrated R–D model. Again, the model captures well the evolution of the experimental measurements over the whole course of the experiment.
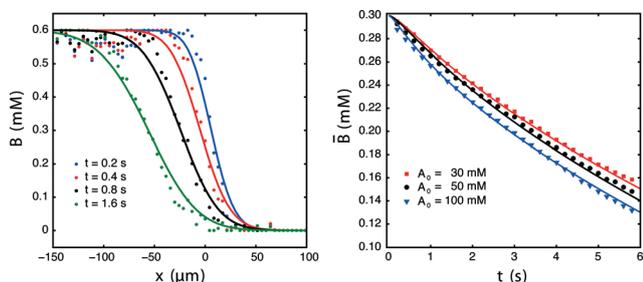
The values of the kinetic constant from the two R–D fitting methods are compared, in Fig. 4, with measurements done in a commercial stopped-flow spectrometer (Biologic Science Instruments) using the same solutions. Since we keep $A_0 \gg B_0$ in our experiments, the process in the well-mixed case behaves as a pseudo-first order reaction[25] and the DCPIP decreases exponentially with time. The characteristic rate of the decay $k_{obs} = kA_0$ is provided directly by the stopped flow apparatus. In the droplet experiments however, the pseudo-first order approximation does not hold since the concentrations of A and B vary in space and time. Instead, the fits with the R–D model yield the value of k. Nonetheless, the measurements in droplets and using the stopped-flow are in very good agreement, as shown in Fig. 4. Indeed, the three methods yield values of k between 80 and 87 M^{-1} s^{-1}, in agreement with previously reported values.[26]

In both the local and integral fitting protocols, k is obtained by finding the minimum of the residual error between the simulations and the experiments (see ESI† sections 3 and 4). The selectivity of these measurements can then be evaluated by observing the behavior of the residual as k departs from the optimal value, particularly while varying the time window in which the fits are performed. We find that a reliable measure of k can be obtained for time windows larger than around 1 s, independently of k_{obs}, and that the selectivity improves for longer windows (ESI† Fig. S3 & S4). This result implies that chemical information can be extracted from the R–D front even at times $t \gg k_{obs}^{-1}$. This contrasts strongly with most approaches in which fast kinetics require a very high time resolution of the measurement method. So while techniques that rely on mixing the species cannot resolve reactions whose typical time is shorter than the mixing time, the droplet-based measurement relies on long observations even for fast kinetics.
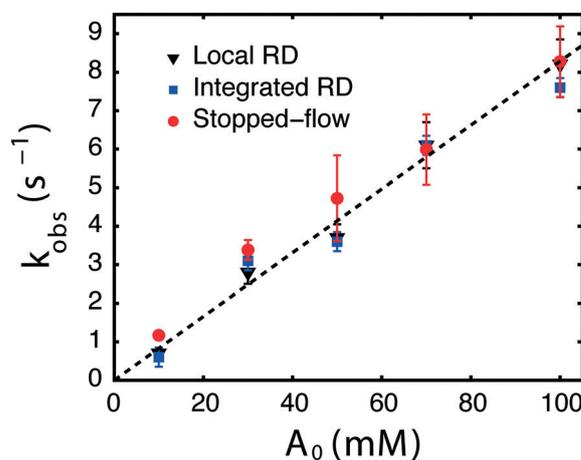

Fig. 4 Comparison between on-chip measurements of k, obtained from spatial and integrated fits, with measurements of $k_{obs} = kA_0$ performed in a stopped-flow spectrometer. $B_0 = 0.6$ mM for all experiments. The error bars on the stopped flow measurement correspond to variations between different runs. The error bars on the reaction–diffusion measurements correspond to the selectivity of the fitting procedure by taking the value of k_{obs} at which the residue increases by 1% from the minimum value.

Fig. 3 (a) Spatial distribution of B and corresponding simulated best fits at different time points. $t = 0$ s is the time of droplet fusion; $x = 0$ μm is the initial position of the fused interface. The initial concentrations are $A_0 = 100$ mM and $B_0 = 0.6$ mM. The solutions are at pH = 6. (b) Evolution of the total amount of B ($\bar{B}$) over time, for three different values of A_0. The solid lines are the best fits obtained from the R–D model.

In practical terms, the results shown here demonstrate that the microfluidic approach can yield equivalent results to the stopped flow apparatus, while using 20 nL of reagents per measurement, compared with typically 100 µL of each reagent per run in the stopped flow. The effective sample consumption is therefore decreased more than 5000 fold. The time required to run these reactions is similar in an automated stopped flow and in the microfluidic system described above. This time can however be greatly reduced by working in a parallelized chip that allows all five conditions of Fig. 4 to be tested on an integrated device. Such a design is shown in Fig. 5 (and ESI† movie S3), where the rail and anchor pattern has been reproduced in order to allow six independent conditions to be tested on a single chip (see ESI† section 5 for chip dimensions).

In this parallel chip, the top row of traps is filled with a single drop of each of the six independent reagents, which originate from different syringes outside the chip (Fig. 5a). Once those positions are occupied (Fig. 5b), six drops of the common reagent are produced on the left hand side, before a gentle flux of oil is used to direct them to the empty trapping sites. It is also possible to use the laser to guide individual droplets into the desired anchors.[17] This leads to all six positions being occupied by six different pairs of drops (Fig. 5c) and the independent reactions can again be triggered, when desired, by the laser.

In conclusion, the method presented here relies on integrating different capabilities on a single chip (drop production and transport, active merging, analysis of the R–D front) to provide a system for measuring fast chemical kinetics while using ultra-low volumes. The fluids are mostly stationary but the geometry and the external flows can be combined to implement temporary movements. Combinatorial assays can thus be obtained by pairing droplets that originate from many different inlets through a pre-programmed sequence of operations. In practice, a few µL of sample are sufficient to run a series of reactions with different substrates in a few minutes. This performance yields significant gains in cost and time, motivating the use of such a device in the screening of molecular interactions or for measuring the kinetics of precious enzymes.

Acknowledgements

References

1 H. Song, D. Chen and R. F. Ismagilov, *Angew. Chem., Int. Ed.*, 2006, **45**, 7336–7356.

2 S.-Y. Teh, R. Lin, L.-H. Hung and A. Lee, *Lab Chip*, 2008, **8**, 198–220.

3 A. B. Theberge, F. Courtois, Y. Schaerli, M. Fischlechner, C. Abell, F. Hollfelder and W. T. S. Huck, *Angew. Chem., Int. Ed.*, 2010, **49**, 5846–5868.

4 N. R. Beer, B. J. Hindson, E. K. Wheeler, S. B. Hall, K. A. Rose, I. M. Kennedy and B. W. Colston, *Anal. Chem.*, 2007, **79**, 8471–8475.

5 A. Hatch, J. Fisher, A. Tovar, A. Hsieh, R. Lin, S. Pentoney, D. Yang and A. Lee, *Lab Chip*, 2011, **11**, 3838–3845.

6 H. N. Joensson and H. Andersson Svahn, *Angew. Chem., Int. Ed.*, 2012, **51**, 12176–12192.

7 D. Chiu, R. Lorenz and G. Jeffries, *Anal. Chem.*, 2009, **81**, 5111–5118.

8 B. Sun, D. Lim, J. Kuo, C. Kuyper and D. Chiu, *Langmuir*, 2004, **20**, 9437–9440.

9 A. Huebner, C. Abell, W. T. S. Huck, C. N. Baroud and F. Hollfelder, *Anal. Chem.*, 2011, **83**, 1462–1468.

10 C. Sims and N. Allbritton, *Lab Chip*, 2007, 7, 423–440.

11 P. Abbyad, R. Dangla, A. Alexandrou and C. N. Baroud, *Lab Chip*, 2011, **11**, 813–821.

12 K. Choi, A. H. Ng, R. Fobel and A. R. Wheeler, *Annu. Rev. Anal. Chem.*, 2012, **5**, 413–440.
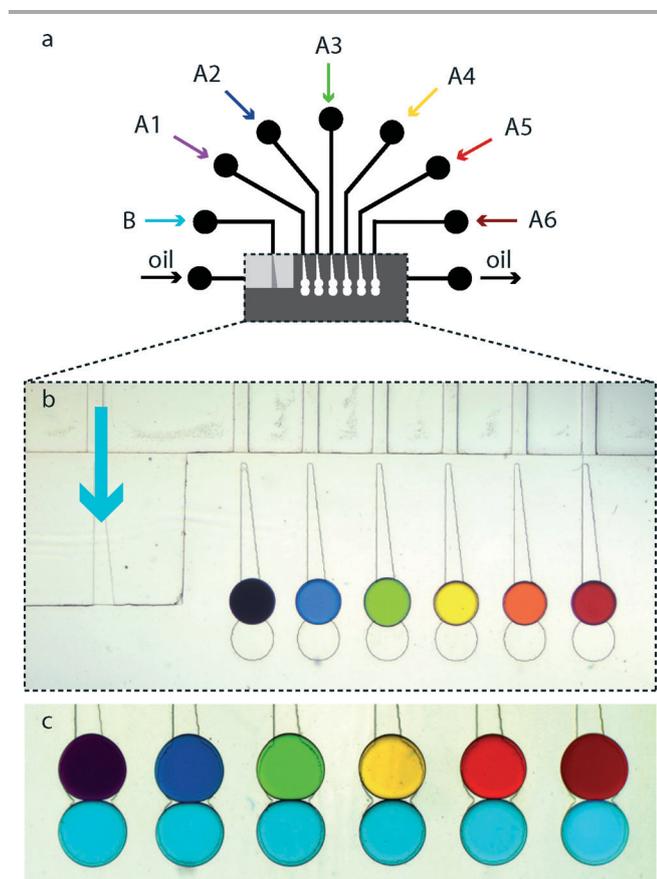

Fig. 5 A parallel chip that serves to test a solution *via* six independent reactions. (a) A sketch of the chip that shows the different inlets. (b) The chip is initially filled with a single droplet of the six test conditions, before the test solution (light blue) is injected from the left-most inlet. (c) After filling, each trap contains a different pair of droplets that can be fused at will by using the focused laser.

13 Y. Bourquin, J. Reboud, R. Wilson, Y. Zhang and J. M. Cooper, *Lab Chip*, 2011, **11**, 2725–2730.

14 C. N. Baroud, F. Gallaire and R. Dangla, *Lab Chip*, 2010, **10**, 2032–2045.

15 R. Dangla, S. Kayi and C. Baroud, *Proc. Natl. Acad. Sci. U. S. A.*, 2013, **110**, 853–858.

16 K. Stephan, P. Pittet, L. Renaud, P. Kleimann, P. Morin, N. Ouaini and R. Ferrigno, *J. Micromech. Microeng.*, 2007, **17**, N69.

17 E. Fradet, C. McDougall, P. Abbyad, R. Dangla, D. McGloin and C. N. Baroud, *Lab Chip*, 2011, **11**, 4228–4234.

18 S. Sugiura, M. Nakajima, S. Iwamoto and M. Seki, *Langmuir*, 2001, **17**, 5562–5566.

19 R. Dangla, E. Fradet, Y. Lopez and C. N. Baroud, *J. Phys. D: Appl. Phys.*, 2013, **46**, 114003.

20 C. Holtze, A. Rowat, J. Agresti, J. Hutchison, F. Angile, C. Schmitz, S. Köster, H. Duan, K. Humphry and R. Scanga, *et al., Lab Chip*, 2008, **8**, 1632–1639.

21 H. Song, J. Tice and R. F. Ismagilov, *Angew. Chem., Int. Ed.*, 2003, **42**, 768–772.

22 X. Niu, S. Gulati, J. Edel and A. de Mello, *Lab Chip*, 2008, **8**, 1837–1841.

23 M. Zagnoni, C. N. Baroud and J. M. Cooper, *Phys. Rev. E*, 2009, **80**, 046303.

24 L. Mazutis and A. D. Griffiths, *Lab Chip*, 2012, **12**, 1800–1806.

25 K. Matsumura, Y. Enoki, H. Kohzuki and S. Sakata, *Jpn. J. Physiol.*, 1990, **40**, 567–571.

26 B. Tonomura, H. Nakatani, M. Ohnishi, J. Yamaguchi-Ito and K. Hiromi, *Anal. Biochem.*, 1978, **84**, 370–383.